Int. J. Electrochem. Sci., 16 **(2021)** Article ID: 210456, doi: 10.20964/2021.04.63

International Journal of
ELECTROCHEMICAL
SCIENCE
www.electrochemsci.org

Synthesis of Rose-Like Sheet Zinc Phosphate by the Induction-Calcination Method and Its Application as a Corrosion Inhibitor in Coatings

Yabo Chen[1,£], *Jihu Wang*[1,£], *Shaoguo Wen*[1,*], *Jijia Zhang*[2], *Xiangyi Yu*[3], *Yan Mao*[3]

[1,2] College of Chemistry and Chemical Engineering, Shanghai University of Engineering Science, Shanghai, 201620, China
[3] Solid Waste and Chemicals Management Center of Ministry of Ecology and Environment, Beijing, 100101, China
[£]These two authors contributed equally to this work and should be considered co-first authors.
[*]E-mail: sgwen1@sues.edu.cn

Received: 18 December 2020 / *Accepted:* 23 February 2021 / *Published:* 28 February 2021

Rose-like sheet zinc phosphate (SZP) was prepared by the induction-calcination method using emulsified paraffin emulsion. The structure of SZP prepared under different conditions was characterized by X-ray photoelectron spectroscopy, X-ray diffractometer, Fourier transform infrared spectroscopy, and Scanning electron microscope. It was added as an anti-corrosive filler to waterborne epoxy-modified acrylic resin. The failure behavior of the coating film was studied by salt spray test and electrochemical workstation. Compared with pure resin, the best neutral salt spray resistance time increased from 24 hours to 336 hours, about 14 times. Besides, the contact angle of the film was measured with a contact angle meter. The results show that SZP can increase the contact angle of the film, improve the water-resistance of the epoxy-modified acrylic resin coating, and prolong the diffusion path of the corrosive medium to the substrate. Therefore, the rose-like sheet zinc phosphate enhances the barrier performance of the coating and can be used as an excellent corrosion inhibitor.

Keywords: Epoxy-modified acrylic resin, Sheet zinc phosphate, Nanomaterials, Coatings, Anti-corrosion

1. INTRODUCTION

Metal corrosion is a common phenomenon in the marine environment [1]. The most common method is to use organic coatings to solve this problem. Epoxy-modified acrylic resin combines the advantages of epoxy resin and acrylic resin, and the cured coating film has the characteristics of high hardness, good gloss, corrosion resistance, heat resistance, and electrochemical properties. It is widely used in the field of anti-corrosion[2-4].

Organic coatings will inevitably have some micropores or defects after film formation[5]. To greatly improve its anti-corrosion ability, it is usually necessary to add some inorganic fillers[6-8]. These fillers can be divided into physical barrier types and chemical reaction passivation types according to their mechanism of action[9]. Common physical barrier types fillers include glass flakes[10], mica iron oxide[11], graphene[12], and other nanosheet materials. Which can delays the path of corrosive media to the substrate, thereby improving the anticorrosive performance of the film[13,14]. The reactive passivation types mainly include phosphate[15], chromate[16], molybdate[17], etc. A dense interface passivation layer is formed through a chemical reaction with the metal substrate. Even if the external film is damaged, the passivation layer can be used as the second barrier to protect the substrate[18]. Both types of fillers exhibit excellent characteristics in the field of anti-corrosion, but physical barrier fillers can only provide passive shielding effects. Once the coating is damaged, the protective function will be lost quickly. Although the chemical reaction passivation type has a better shielding and protection effect, it cannot be ignored that the product after the reaction will cause certain pollution to the environment. For example, chromate has greater biological toxicity[19]. Therefore, it is very important to design a non-toxic and green material, which can react with the substrate to form a complex film. The advantages of non-toxic and environmentally friendly phosphates are highlighted, and zinc phosphate is the most widely used[20,21].

The common microscopic morphologies of zinc phosphate are hollow and sheet structure[22]. Zinc phosphate hollow microspheres are usually loaded or grafted with some organic corrosion inhibitors or hydrophobic agents to improve the anti-corrosion performance [23], and the synthesis process is relatively complicated. Moreover, when the organic matter is exhausted, the film will cause micro-pores in the microscopic view, destroy the integrity of the coating, and reduce the corrosion inhibition performance of the coating[24,25]. Therefore, the sheet structure filler is more advantageous than the spherical shape in remedying these defects.

As far as we know, there is no report on the synthesis of sheet zinc phosphate (SZP) with emulsified paraffin as the inducer. In this work, emulsified paraffin was used as an inducer, combined with calcination to synthesize a rose-like sheet zinc phosphate. The formation mechanism is also given. Besides, electrochemical impedance spectroscopy (EIS) was used to study its anti-corrosion mechanism in the coating.

2. EXPERIMENTAL

2.1 Chemicals

Disodium hydrogen phosphate(Na_2HPO_4), Zinc nitrate hexahydrate ($Zn(NO_3)_2 \cdot 6H_2O$), and Ammonia solution 25% were obtained by Sinopharm Chemical Reagent Co., Ltd. (Shanghai, China). Anhydrous ethanol was got from Aladdin Reagent Co., Ltd. (Shanghai, China). Emulsified paraffin (lw-02, pH 7-9, Solid content 45wt%) was purchased from Nanjing Tianshi New Material Technology Co., Ltd. (Nanjing, China). Deionized water (H_2O) was used in all experiments. The waterborne epoxy-modified acrylic resin was supplied by Qixiang Qingchen Materials Technology Co., Ltd. (Shanghai, China).

2.2 Synthesis of sheet zinc phosphate

The sheet zinc phosphate was synthesized by the induction-calcination method. In the first step, 0.3 mmol $Zn(NO_3)_2 \cdot 6H_2O$ was dissolved in 100 mL H_2O, and then added the paraffin emulsion(lw-02) to the prepared zinc nitrate solution and fully stirred, and set aside; In the second step, 0.2 mmol Na_2HPO_4 was added to 100 mL H_2O and stir well to dissolve, and then added to the solution prepared in the first step, adjusted to pH=8 with ammonia, and treated with ultrasound for 20 minutes. Thirdly, it was transferred to a constant temperature water bath at 50°C, with a magnetic stirring speed of 30 rpm for 2 hours, aged at 40℃ for 8 hours, centrifuged several times, and washed with ethanol. Finally, it was dried at 40°C, and ground to obtain the sheet zinc phosphate (SZP). In the stage of zinc phosphate synthesis, the effect of different content of emulsified paraffin wax (lw-02) on the morphology of zinc phosphate was mainly studied. SZP (0wt% lw-02) means that no emulsified paraffin wax is added during the synthesis process; SZP (0.5wt% lw-02) and SZP (1.0wt% lw-02) means that the emulsified paraffin wax is added in the synthesis process at 0.5wt% and 1wt%; SZP (1.0wt% lw-02 300°C) means that the SZP (1.0wt% lw-02) was treated at 300° C for 2hours. The percentage of emulsified paraffin refers to the weight percentage in 100mL of deionized water.

2.3 Preparation of SZP/epoxy modified acrylic resin coating

Rose-like SZP (1.0wt% lw-02 300℃) was added to the waterborne epoxy modified acrylic (50g) resin in different proportions (0.1wt%, 0.3%, 0.5wt%, 0.7wt% and 0.9wt%) and stirred for 2 hours. Subsequently, the SZP/epoxy-modified acrylic resin coating was applied to the tinplate substrate with a wet film maker and cured for 7 days at room temperature. The thickness of the film is controlled at 35±5μm. The SZP/epoxy modified acrylic resin coatings with different addition amounts is represented by pure resin, 0.1wt% SZP, 0.3wt% SZP, 0.5wt% SZP, 0.7wt% SZP and 0.9wt% SZP.

2.4. Characterizations

The characteristic functional groups of SZP were characterized by FT-IR and tested in ATR mode (PerkinElmer, MA). The crystal structure of SZP was characterized by XRD (Bruck GmbH, Germany). The surface chemical element of SZP was characterized by XPS with an Al Kα X-ray source (Thermo Escalab 250XI). The morphology of SZP was observed by SEM (SU8010, Hitachi Co, Japan). The hydrophilic and hydrophobic state of the coating surface is measured with a contact angle meter (CA Goniometer 190-F2, Rame-hart, USA). The salt spray resistance of the coating was tested by a precision salt spray test machine (Shanghai Keheng Testing Instrument Co., Ltd.). Electrochemical corrosion behavior is measured by an electrochemical workstation (CHI660E, Shanghai Chenhua Device Co., Ltd.).

3. RESULTS AND DISCUSSION

3.1 Characterization of SZP

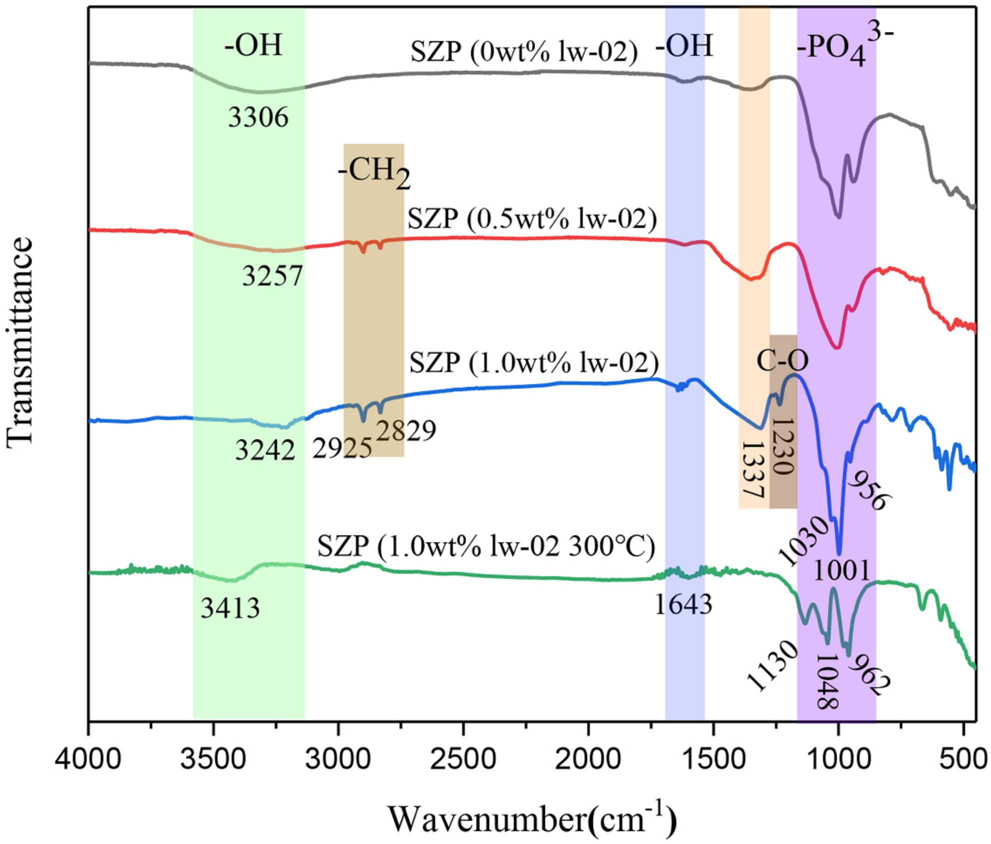

Figure 1. FT-IR spectra of SZP under different conditions.

The FT-IR spectra of SZP prepared by adding different amounts of emulsified paraffin wax (lw-02) are shown in **Fig. 1**. The stretching vibration absorption peak of -OH at 3600-3000 cm^{-1}[26]. The absorption peak at 1643 cm^{-1} is attributed to the H-O-H, confirming the presence of crystal water in the SZP [27,28]. The stretching and vibration absorption peaks of the PO_4^{3-} group correspond to multiple absorption peaks at 1200 ~ 940 cm^{-1} and 640 ~ 630 cm^{-1}[29]. The absorption peaks of -CH_2 at 2925 and 2829 cm^{-1}, and the absorption peak at 1230 cm^{-1} corresponds to the C-O bond, which proves the existence of organic emulsified paraffin. After calcination at 300°C, the -OH peak becomes weaker, indicating that the free water on the surface has decreased. The absorption peak at 1643 cm^{-1} may be attributed to the secondary crystallization after drying. The increase of PO_4^{3-} group peak intensity may be attributed to the increase of crystallinity at high temperatures. Therefore, the infrared spectrum analysis shows that SZP was successfully prepared.

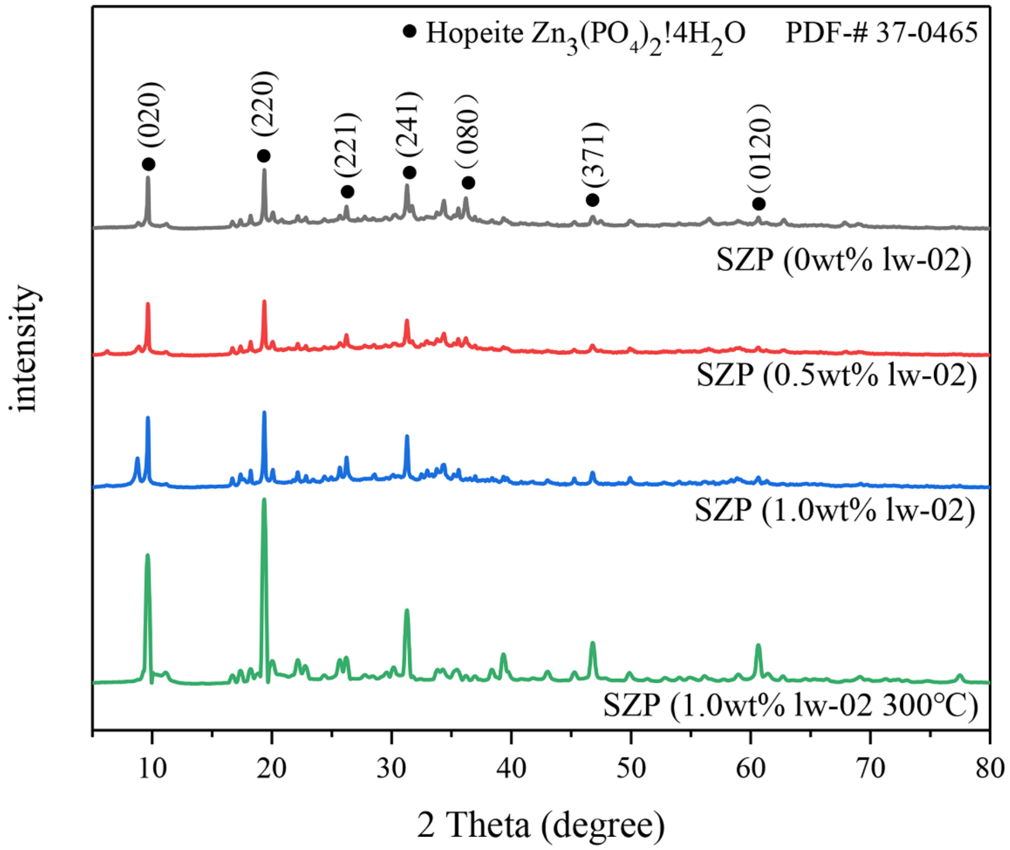

Figure 2. XRD pattern of SZP under different conditions.

The XRD pattern of the synthetic SZP is shown in Fig 2. The diffraction peak of SZP matches the standard spectrum information of $Zn_3(PO_4)_2·4H_2O$ (PDF-# 37-0465). According to the characteristic pattern, When the addition amount of emulsified paraffin (lw-02) is 0.5wt% and 1.0wt%, it is the same as the crystal form of pure zinc phosphate, indicating that the intervention of emulsified paraffin has little effect on its crystal form. When SZP (1.0wt% lw-02 300℃) was calcined at 300°C, the diffraction peak intensity at 9.69°, 19.42°, 26.28°, 31.33°, 39.37°, 46.81° and 60.65° was found to increase, indicating that secondary crystallization occurred during the calcination process, which increased the crystallinity.

The elemental composition and surface chemical states of the as-synthesized SZP (1.0wt% lw-02 300℃) were analyzed using XPS.

The result of a wide-scan survey from Fig. 3a shows that the signals of Zn, P, C, and O elements can be identified. Fig. 3b shows the spectrum of O1s in SZP. The binding energies at 532.25 eV and 531.4 eV are ascribed to the O-P-O bond and the hydroxide component in SZP. Fig. 3c shows the spectrum of P 2p in SZP. The binding energies of the O-P-O bond in the (PO_4) structure are located at 133.4 eV (P $2p_{1/2}$) and 134.2 eV (P $2p_{2/3}$)[30]. Fig. 3d shows the spectrum of Zn 2p in SZP. It can be seen that the binding energies at 1022.6 eV and 1045.6 eV, which belonged to Zn $2p_{3/2}$ and Zn $2p_{1/2}$, respectively[31]. Through XPS analysis combined with infrared spectroscopy and XRD, it can be confirmed that SZP materials have been successfully prepared.

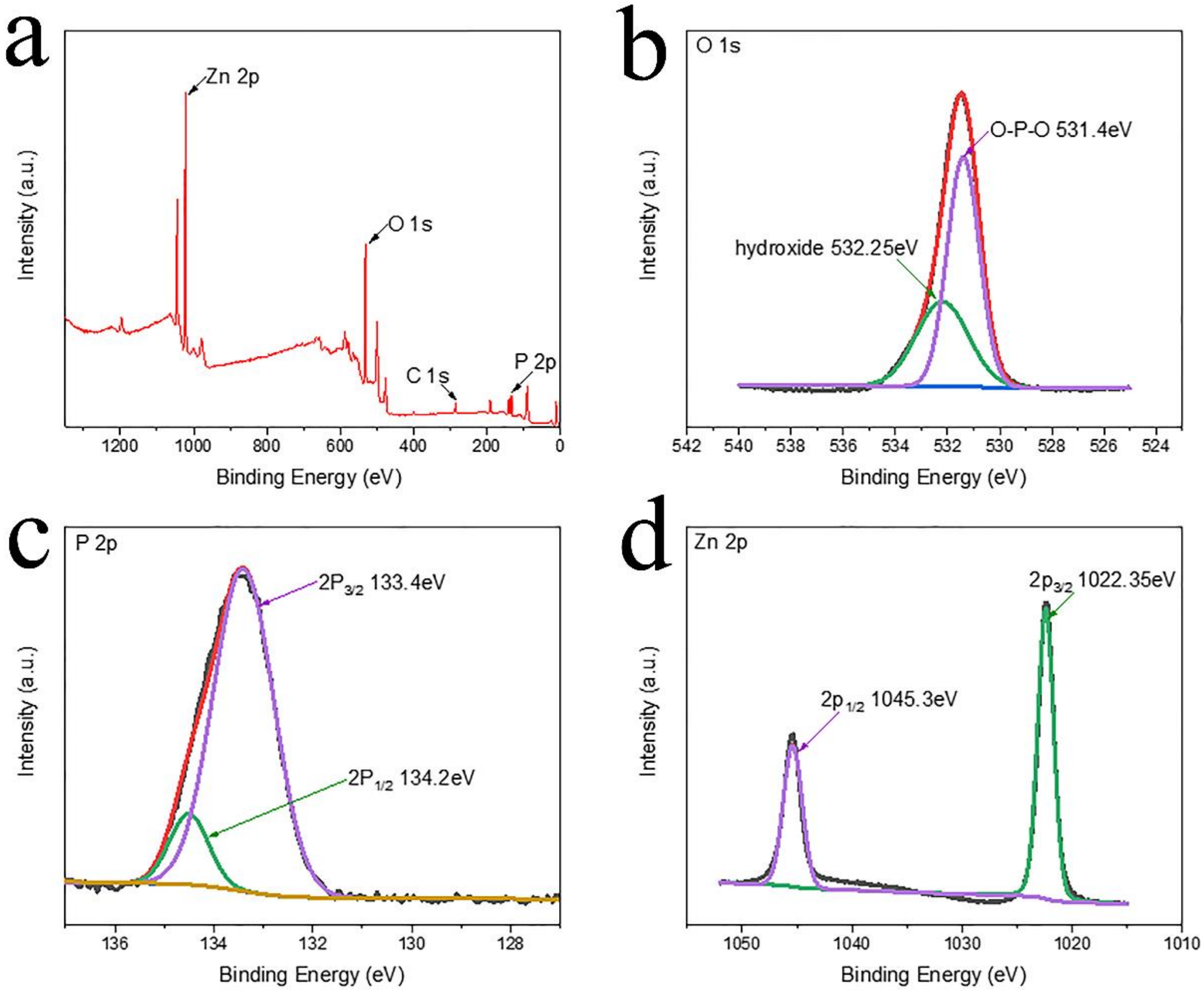

Figure 3. XPS spectra of (a) SZP(1.0wt% lw-02 300℃), (b)O 1s, (c)P 2p and (d)Zn 2p.

Fig. 4 illustrates the SEM morphology of SZP without and with emulsified paraffin. In the absence of emulsified paraffin, the shape of SZP is amorphous agglomerated nanoparticles, as shown in Fig. 4 (a-b). It can be seen from Fig. 4 (c-d), sheet layers of SZP gradually appear when the addition amount is 0.5wt% compared with no emulsified paraffin is added. As shown in Fig. 4 (e-f), when the addition amount of emulsified paraffin reached 1.0wt%, the sheet structure is increased and the surface is smooth. The size is about 200-500 nm, and the thickness is below 30 nm, which is smaller and thinner than that of using the surfactant PEG2000 reported in the literature[9]. This shows that emulsified paraffin plays a key role in the formation of sheet zinc phosphate products. After calcining at 300℃ for 2h, the product image is shown in Fig. 4(g-h). A peculiar rose-like structure was found, which has a larger specific surface area than a simple sheet. It is an ideal corrosion inhibitor in the field of anti-corrosion.

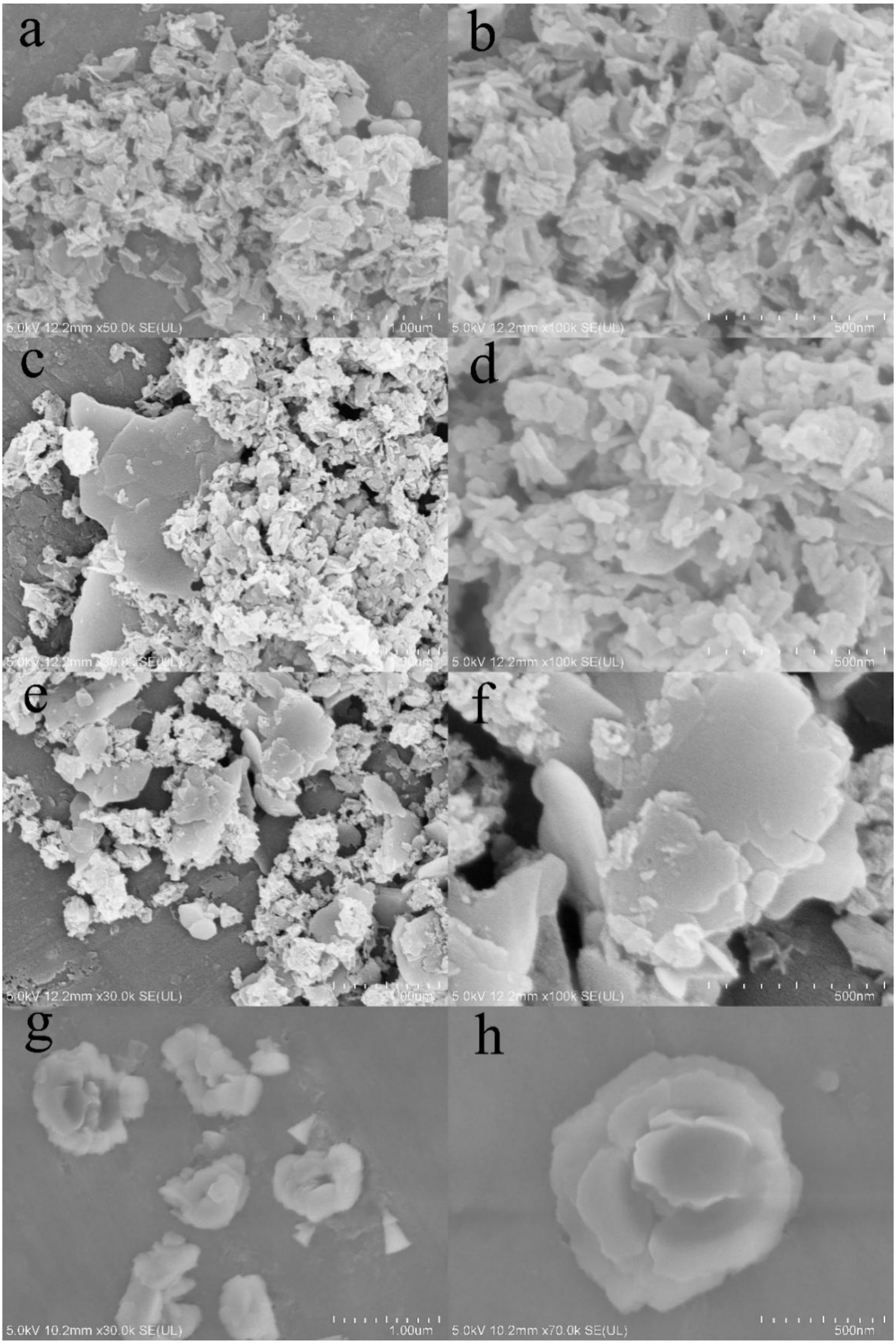

Figure 4. SEM images of SZP under different conditions. (a-b) SZP(0wt% lw-02), (c-d) SZP(0.5wt% lw-02), (e-f) SZP(1.0wt% lw-02), (g-h) SZP(1.0wt% lw-02 300℃)

3.2 The formation mechanism of sheet zinc phosphate

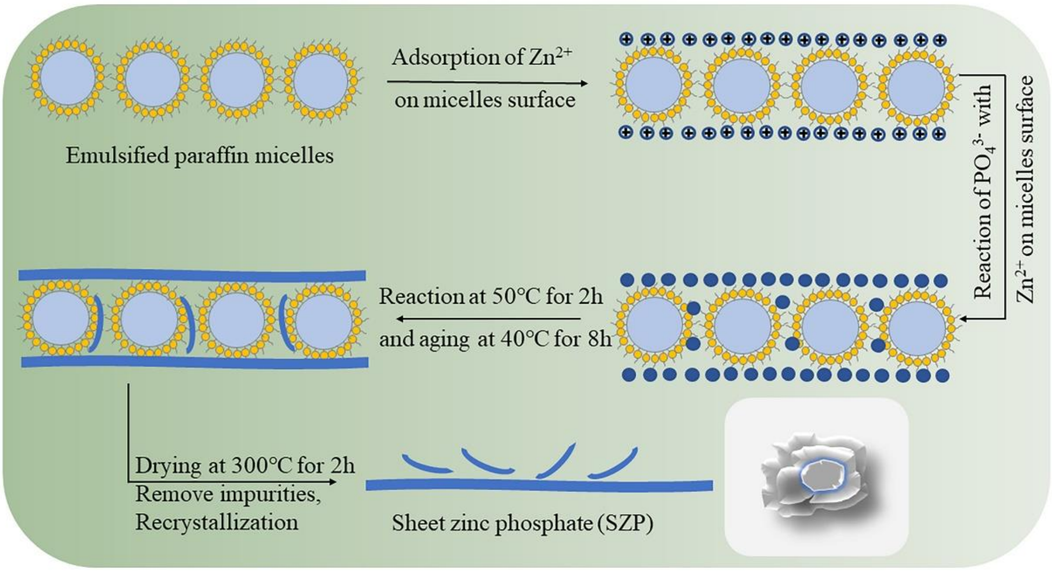

Figure 5. Diagram of the formation mechanism of prepared SZP(1.0wt% lw-02 300°C)

Based on the observation and characterization of synthetic materials, the mechanism of the formation of rose-like sheet-layer zinc phosphate particles was discussed. As shown in Fig. 5, because the emulsified paraffin wax is electronegative, Zn^{2+} are first adsorbed on the emulsified paraffin particles. The presence of emulsifiers makes the latex particles stable, so the zinc ions are ordered and stable. When the phosphate ion intervenes, it reacts with zinc ions to became zinc phosphate. The zinc phosphate formed at this time is arranged on the surface of the micelles. The emulsified paraffin volatilized during the calcination process at 300°C, the zinc phosphate then migrated and crystallized again, and finally showed a rose-like sheet zinc phosphate product.

3.3 Wettability of different coatings

Through the static contact angle test of water on the coating, It is found that adding different quality of SZP can improve the contact angle, which can reach about 90°. The coating state tends to change from hydrophilic to hydrophobic.

Generally speaking, the larger the static contact angle, the more hydrophobic the coating[32]. It shows that the introduction of SZP is more conducive to preventing corrosive media (such as chloride ions, water, and solvents) from penetrating the metal substrate through the film, thereby improving the protection ability. In a sense, it also has a certain positive meaning for the initial waterproofness of the film[33].

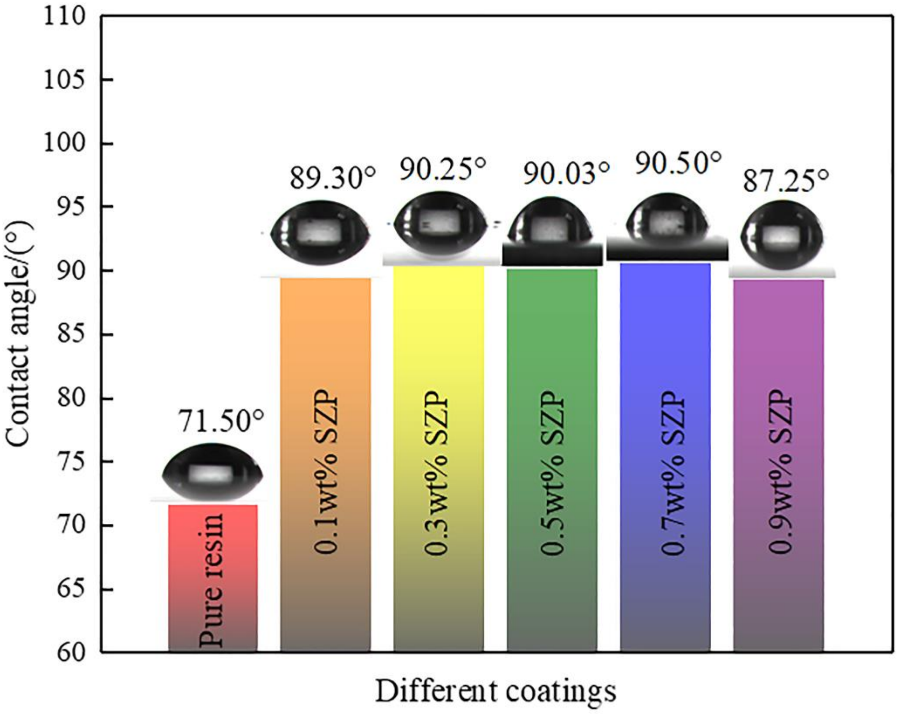

Figure 6. The water contact angle of different coatings

3.4 Electrochemical impedance spectroscopy (EIS) test

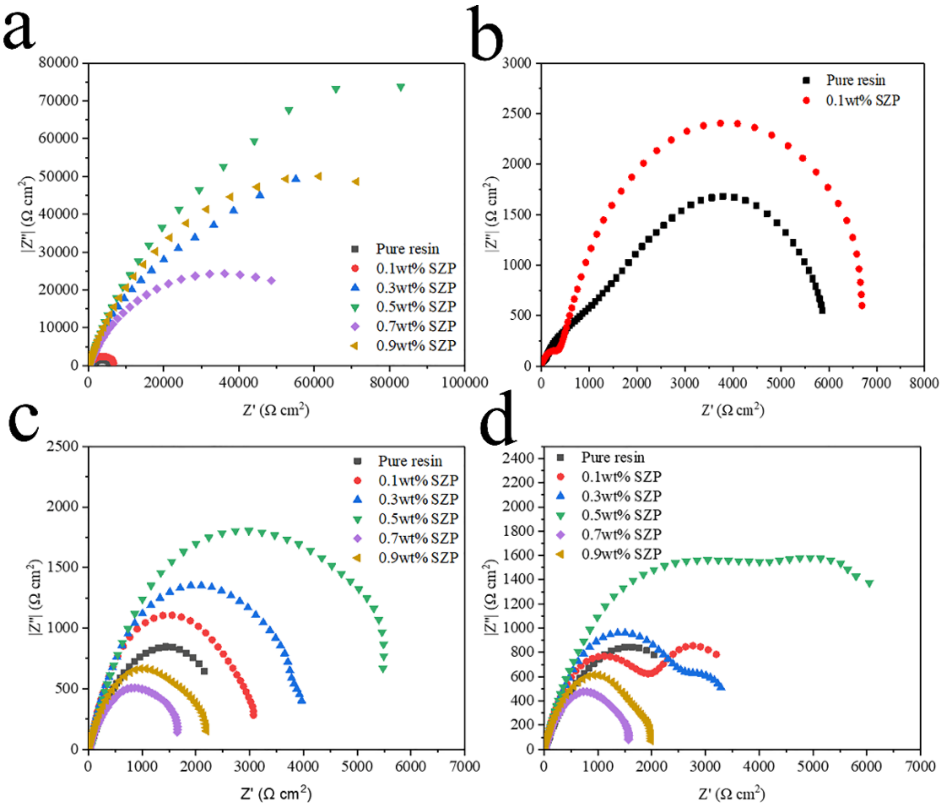

Figure 7. Nyquist plots of different coatings at different immersion times (a-b) 3 h, (c) 24 h, (d) 72 h.

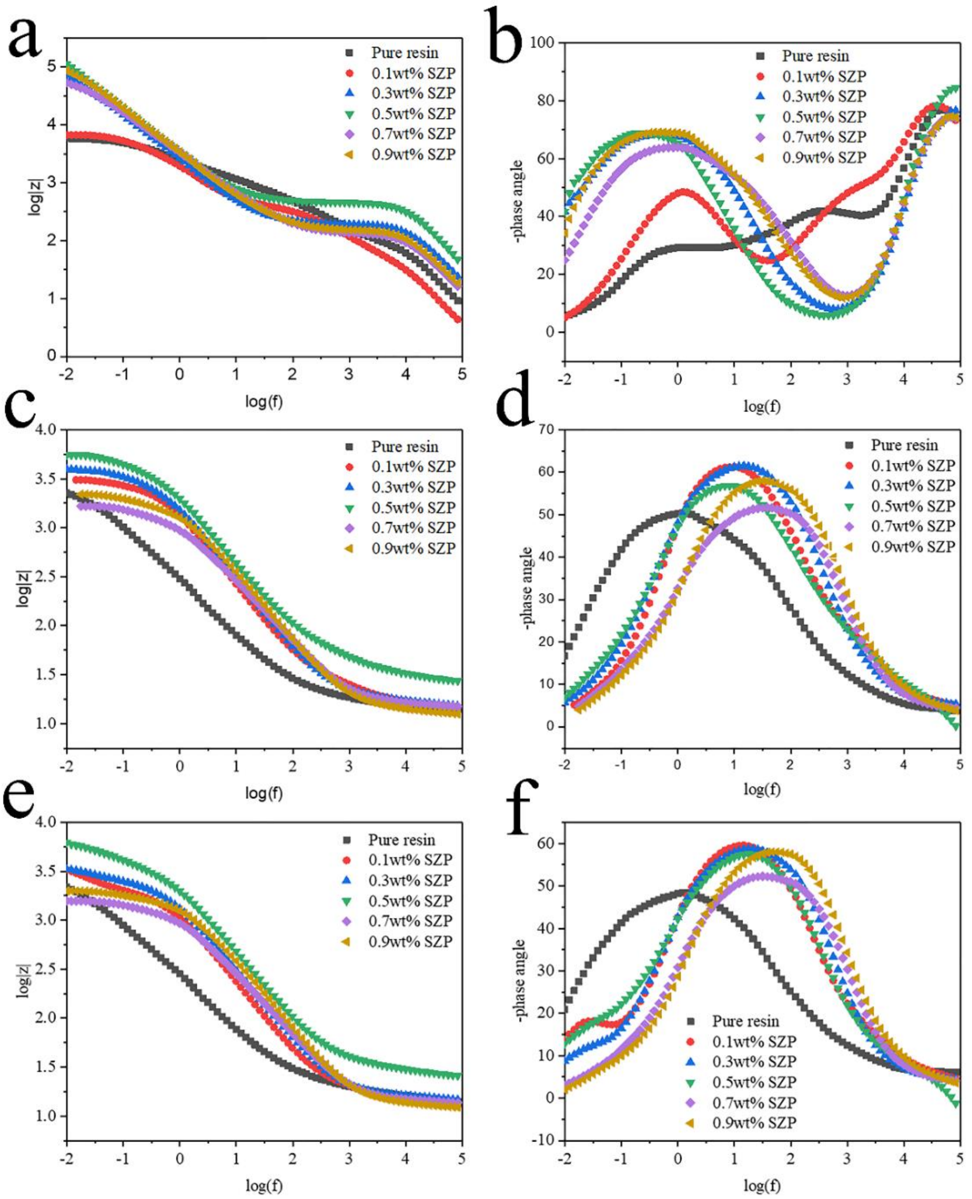

Figure 8. Bode plots of different coatings at different immersion times (a-b) 3 h, (c-d) 24 h, (e-f) 72 h.

EIS is an effective method for studying the corrosion behavior of metals[34]. The EIS test data of the coating can be characterized by Bode and Nyquist plots, and the failure process of the coating can be obtained by analyzing these diagrams.

Figs. 7 and 8 respectively show the Nyquist and Bode plots of different coatings immersed in 3.5wt% NaCl solution at room temperature. The resistance value of the different coating shows a decreasing trend as the immersion time increases. Capacitor arc and the lowest frequency impedance are the two most important parameters for EIS[35]. Fig. 7 (a, b) and Fig. 8a reveal that after immersing for 3 hours, the capacitance arc and low frequency impedance value of the epoxy modified acrylic resin coating added SZP has been increased. It shows that after adding SZP, the protective ability of the coating is improved to a certain extent, and the coating is most prominent when 0.5wt% SZP is added.

After being immersed for 24 and 72 hours, low-frequency impedance value and capacitance arc of the coating are decreased, which means that water, oxygen, ions, etc. have penetrated the film and corroded the substrate at this time. However, when the addition amount of SZP is 0.1wt%, 0.3wt%, 0.5wt%, there is still a larger capacitance arc and low-frequency impedance value than pure coating. It reveals that the barrier function of SZP coating is excellent even after the corrosive medium reaches the substrate. When the addition amount of SZP is 0.7wt% and 0.9wt%, the capacitance arc decreases. This due to the accumulation of excessive SZP, which causes local agglomeration inside the film and reduces the later corrosion resistance. Therefore, it shows that the addition amount is also an extremely important factor in terms of anti-corrosion performance.

In addition, the phase angle is also a key indicator to judge the protective effect of the film[36]. When the phase angle in the Bode diagram is closer to 90°, the coating protection performance will be better. As shown in Fig. 8 (b, d, f), the phase angle of the coatings added with SZP are higher than that of the pure coating as the immersion time increases. Therefore, the SZP can effectively improve the barrier ability of epoxy-modified acrylic resin coating.

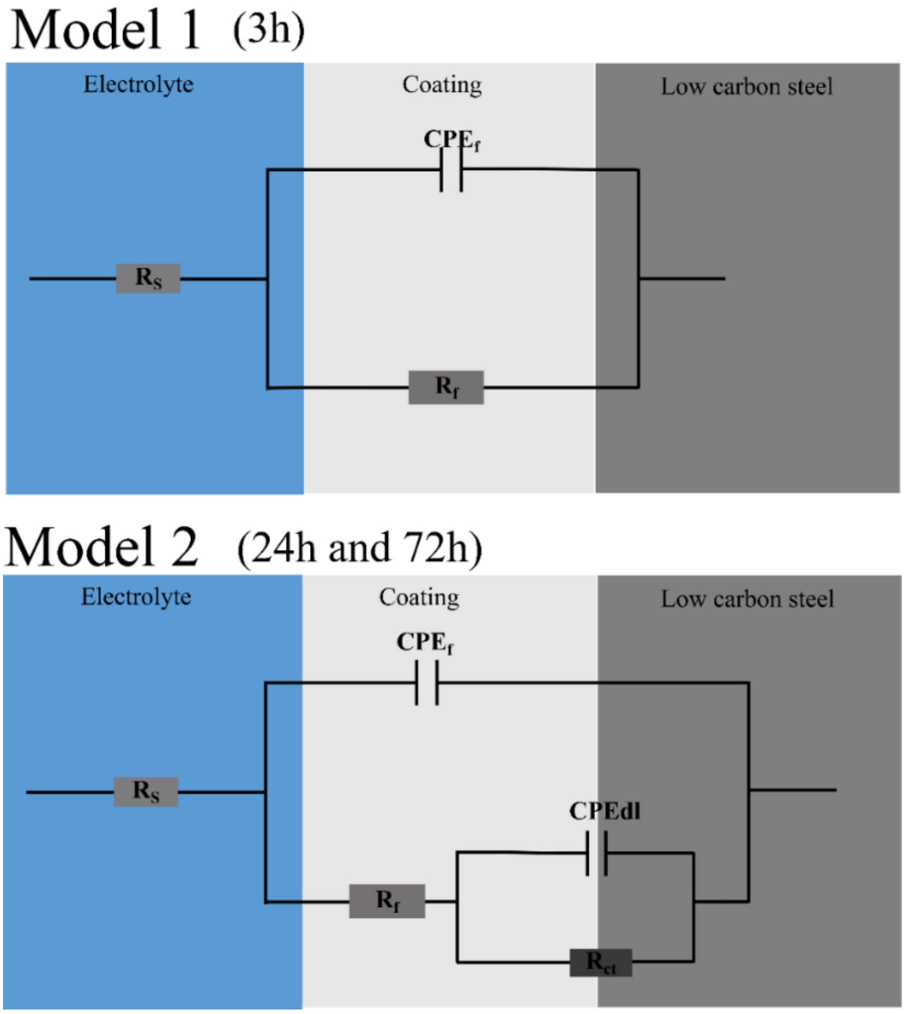

Figure 9. Equivalent circuit models in different periods

Table 1. Fitting data of EIS of different coatings.

Coatings	Time(h)	$R_s(\Omega\ cm^2)$	$CPE_f(F/cm^2)$	$R_f(\Omega\ cm^2)$
Pure resin	3	15.52	3.10×10^{-6}	4306
0.1wt% SZP	3	36.99	6.67×10^{-5}	5592
0.3wt% SZP	3	22.65	5.63×10^{-5}	63170
0.5wt% SZP	3	53.55	5.19×10^{-5}	106200
0.7wt% SZP	3	17.61	3.42×10^{-5}	43310
0.9wt% SZP	3	19.43	3.81×10^{-5}	79860

R_s-solution resistance, CPE_f- film capacitance, R_f- film resistance.

Table 2. Fitting data of EIS of different coatings.

Coatings	Time(h)	$R_s(\Omega\ cm^2)$	$R_f(\Omega\ cm^2)$	$CPE_f(F/cm^2)$	$R_{ct}(\Omega\ cm^2)$	$CPE_{dl}(F/cm^2)$
Pure resin	24	14.52	60.09	1.04×10^{-3}	2940	3.27×10^{-5}
	72	14.69	48.10	1.21×10^{-3}	2230	5.29×10^{-5}
0.1wt% SZP	24	15.22	68.08	1.41×10^{-4}	3191	1.74×10^{-5}
	72	14.00	24.05	1.92×10^{-4}	1305	7.52×10^{-2}
0.3wt% SZP	24	15.49	86.27	1.41×10^{-4}	4120	6.95×10^{-6}
	72	14.44	51.72	1.65×10^{-4}	3206	9.83×10^{-6}
0.5wt% SZP	24	28.13	173.70	1.19×10^{-4}	6010	8.74×10^{-6}
	72	25.17	60.79	1.20×10^{-4}	6163	6.01×10^{-6}
0.7wt% SZP	24	14.30	71.06	1.75×10^{-4}	1791	4.27×10^{-6}
	72	13.40	50.17	2.15×10^{-4}	1290	1.39×10^{-2}
0.9wt% SZP	24	12.89	39.94	1.21×10^{-4}	1978	5.77×10^{-3}
	72	11.74	29.85	1.24×10^{-4}	1278	4.38×10^{-3}

R_s-solution resistance, CPE_f- film capacitance, R_f- film resistance, CPE_{dl}-coating capacitance, R_{ct}-charged transfer resistance.

To further explore the anti-corrosion performance of the coating, the equivalent circuit was used to fit the EIS data as shown in Fig. 9. Corrosion parameter data after fitting are shown in Table 1 and Table 2. When the coating is just immersed in the sodium chloride solution, the organic coating can be regarded as a large resistance and has the best protective effect at this time. Adopt model 1 in Fig. 9 to describe this process. Therefore, the film resistance (R_f) is an extremely important indicator. The data in Table 1 shows that the coating has the highest film resistance when the SZP addition is 0.5wt%, indicating that the film has the best anti-corrosion performance.

As the immersion time increases, water, oxygen, ions, etc. reaches the surface of the metal along with occurring the micropores in the film. Adopt model 2 in Fig. 9 to describe this process[37]. The most intuitive thing is the change in corrosion parameters. R_{ct} represents the electron transfer activity at the interface between the coating and the metal[38], which can indirectly reflect the corrosion resistance of the coating. The larger the value, the better the corrosion resistance [39]. The data in Table 2 shows that the 0.5wt% SZP coating has the highest R_{ct} value after being immersed for 24h and 72h. Compared with pure epoxy-modified acrylic resin coating, the R_{ct} value increased from 2230 F/cm^2 to 6163F/cm^2.

The water absorption capacity of the film is related to CPE_f, and the increase of the CPE_f value means that the moisture inside the coating is enriched[40]. Therefore, the smaller the CPE_f value, the smaller the fluctuation with the immersion time, the stronger the barrier ability of the coating. It can be seen that after 72 hours of soaking, the CPE_f value of 0.5wt% SZP coating is the smallest, indicating that 0.5wt% SZP coating has a stable internal structure and unique compactness.

CPE_{dl} represents the double-layer capacitance at the coating/substrate interface, its value can reflect the stability and compatibility of the coating/substrate interface[41]. The smaller the fluctuation of CPE_{dl} value with the immersion time, the stronger the protective ability of the coating. The data in Table 2 shows that 0.5wt% SZP coating has the lowest CPE_{dl} value ($6.01\times10^{-6}F/cm^{-2}$) and a relatively stable value, which means the good compatibility of 0.5wt %SZP coating with the substrate. In summary, the introduction of SZP filler greatly improves the comprehensive protective ability of epoxy-modified acrylic resin coating, and the effect is most prominent when the addition amount is 0.5wt%.

3.5 Salt spray measurement

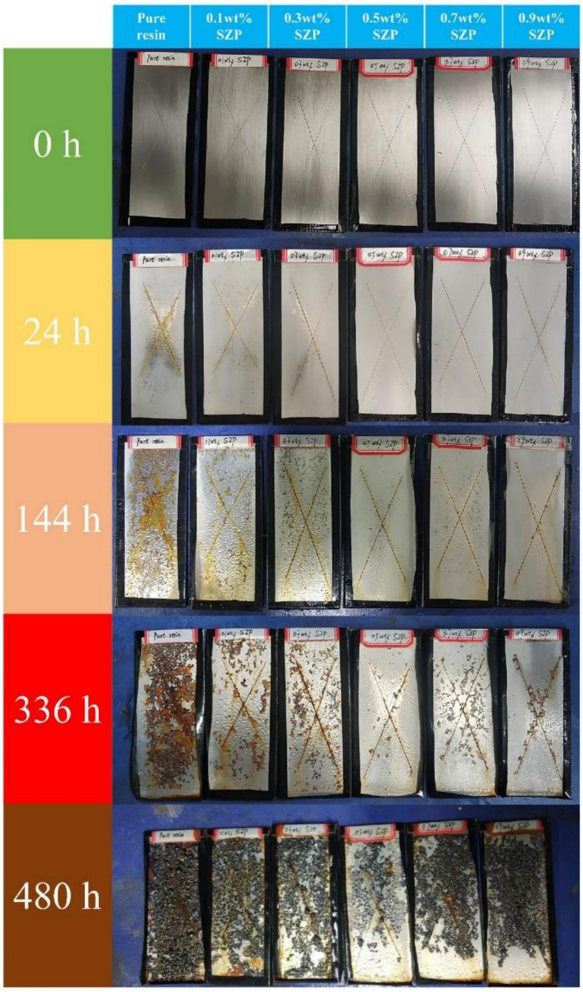

Figure 10. Neutral salt spray test results of different coatings at different times

The most direct way to verify the anti-corrosion performance of the coating is the salt spray test[42,43]. Fig. 10 shows the neutral salt spray test results of pure resin and SZP coating at different times. After being exposed 24 hours, the pure resin coating and addition amount of 0.1wt%, 0.3wt% SZP coating scratches appeared blisters. The pure resin coating was the most serious, and appeared sporadic rust spots. After being exposed 144 hours, the order of severity of corrosion is as follows: pure resin coating>0.1wt% SZP coating>0.3 wt% SZP coating>0.7 wt% SZP coating>0.9 wt% SZP coating Layer>0.5 wt% SZP coating. When exposed 336 hours, all coatings showed corrosion and blisters, but no rust occurred at the blisters of 0.5wt% SZP coating, indicating that the passivation film formed by zinc phosphate and iron played a good role in the protective effect. When the film was exposed 480 hours, the 5wt% SZP coating was not completely corroded compared to other coatings. Therefore, it can be concluded that the best addition amount of SZP coating is 0.5wt%, and the best neutral salt spray resistance time is 336 hours. It is increased by 14 times compared with pure resin.

3.6 Corrosion protection mechanism

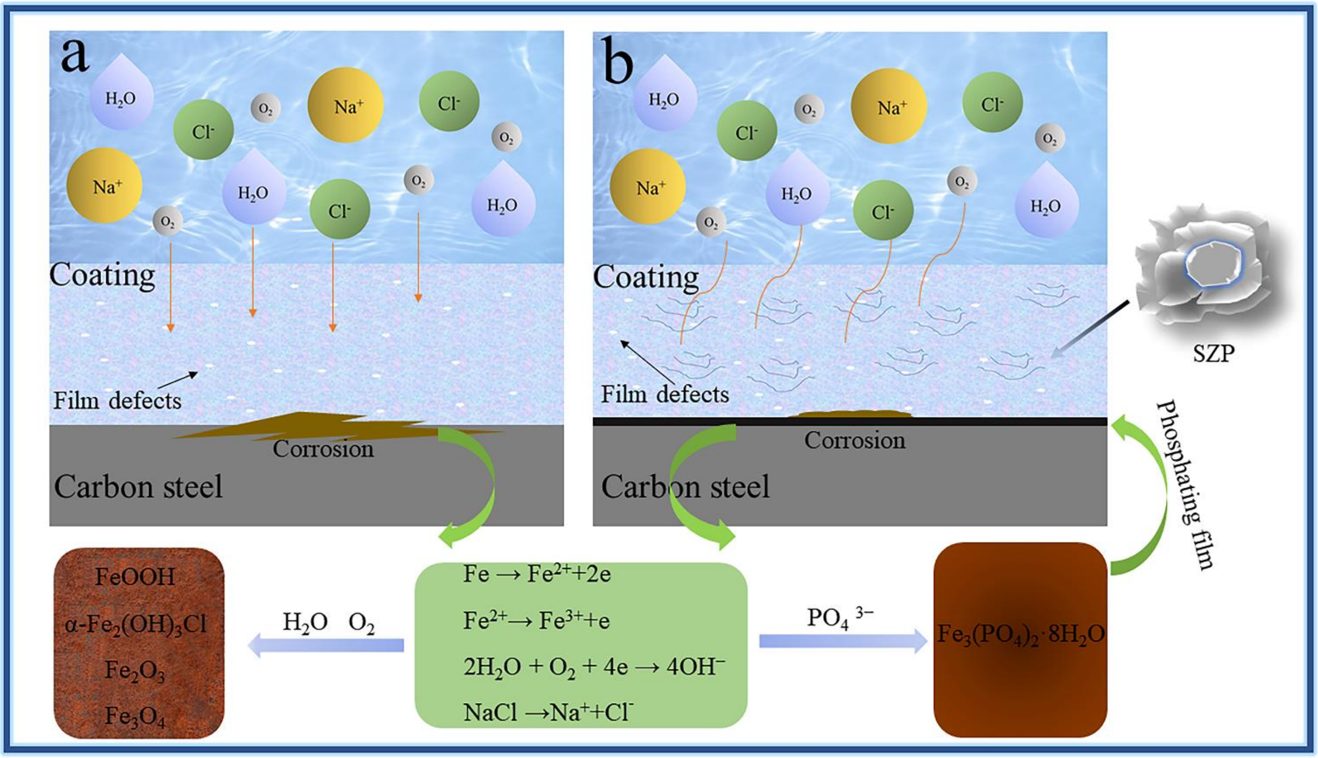

Figure 11. Corrosion mechanism diagrams of (a) Epoxy modified acrylic resin coating, (b) Epoxy modified acrylic resin /SZP coatings

After a series of studies, the anti-corrosion mechanism of different coatings is proposed as shown in Fig. 11. For the pure waterborne epoxy-modified acrylic system (Fig. 11a), due to the hydrophilic and micropores due to the stress shrinkage during film formation, the corrosive medium easily penetrates film. If there is an intrusion of external corrosive media, a series of electrochemical and redox reactions will occur at the interface, cause the coating to gradually fail. As shown in Fig. 11b, SZP forms a multilayer arrangement in the coating, thereby enhancing the barrier effect of the coating. At the same time, as a corrosion inhibitor, SZP can react with the iron matrix to form an iron phosphate film, which increases the number of coating layers and film resistance.

4. CONCLUSION

In short, a rose-like sheet zinc phosphate filler was successfully prepared by the induction-calcination method. SEM observation shows that the synthesized SZP has a rose-like structure, which specific surface area is larger than pure sheet zinc phosphate. As a functional filler, rose-like SZP can further increase the water contact angle and service life of the epoxy-modified acrylic coating. EIS test results prove that the coating has the best anti-corrosion performance when the addition amount of SZP is 0.5wt%. The neutral salt spray experiment proves that the coating filled with SZP has an excellent function of blocking corrosive media and effectively protects the metal substrate. Compared with pure resin, the best neutral salt spray resistance time is increased from 24h to 336h, about 14 times. Therefore, as a micro-nano material, the SZP(1.0wt% lw-02 300℃) prepared in this paper has excellent barrier properties that can effectively inhibit the penetration of corrosive electrolytes to achieve long-term protection, and has broad application prospects in the protection of metal equipment.

ACKNOWLEDGMENTS
Grand science and technology special project supported by the Science and Technology Ministry of China (Grant number 2018YFC1801503)

References

1. R. Kuruvila, S. Thirumalai Kumaran, M.A. Khan, M. Uthayakumar, *Corros. Rev.*, 36 (2018) 435–447. https://doi.org/10.1515/corrrev-2018-0022.
2. Y. Hao, F. Liu, E.-H. Han, *Prog. Org. Coatings.*, 76 (2013) 571–580. https://doi.org/10.1016/j.porgcoat.2012.11.012.
3. F.-L. Jin, X. Li, S.-J. Park, *J. Ind. Eng. Chem.*, 29 (2015) 1–11. https://doi.org/10.1016/j.jiec.2015.03.026.
4. D. Nguyen Thuy, H. To Thi Xuan, A. Nicolay, Y. Paint, M.-G. Olivier, *Prog. Org. Coatings.*, 101 (2016) 331–341. https://doi.org/10.1016/j.porgcoat.2016.08.021.
5. Y. He, W. Xu, R. Tang, C. Zhang, Q. Yang, *RSC Adv.*, 5 (2015) 90609–90620. https://doi.org/10.1039/C5RA19296J.
6. B.-E. Gu, C.-Y. Huang, T.-H. Shen, Y.-L. Lee, *Prog. Org. Coatings.*, 121 (2018) 226–235. https://doi.org/10.1016/j.porgcoat.2018.04.033.
7. A. El-Faham, A.M. Atta, S.M. Osman, A.O. Ezzat, A.M. El-saeed, Z.A. AL Othman, H.A. Al-Lohedan, *Prog. Org. Coatings.*, 123 (2018) 209–222. https://doi.org/10.1016/j.porgcoat.2018.07.006.
8. J.R. Vilche, E.C. Bucharsky, C.A. Giúdice, *Corros. Sci.*, (2002). https://doi.org/10.1016/S0010-938X(01)00144-5.
9. C. Shi, Y. Shao, Y. Wang, G. Meng, B. Liu, *Prog. Org. Coatings.*, 117 (2018) 102–117. https://doi.org/10.1016/j.porgcoat.2018.01.008.
10. J. González-Guzmán, J.J. Santana, S. González, R.M. Souto, *Prog. Org. Coatings.*, 68 (2010) 240–243. https://doi.org/10.1016/j.porgcoat.2010.01.005.

11. T. Liu, Y. Liu, Y. Ye, J. Li, F. Yang, H. Zhao, L. Wang, *Prog. Org. Coatings*., 132 (2019) 455–467. https://doi.org/10.1016/j.porgcoat.2019.04.010.
12. W. Wang, H. Wang, J. Zhao, X. Wang, C. Xiong, L. Song, R. Ding, P. Han, W. Li, *Chem. Eng. J*., 361 (2019) 792–804. https://doi.org/10.1016/j.cej.2018.12.124.
13. W. Tian, L. Liu, F. Meng, Y. Liu, Y. Li, F. Wang, *Corros. Sci*., 86 (2014) 81–92. https://doi.org/10.1016/j.corsci.2014.04.038.
14. M. Ganjaee Sari, B. Ramezanzadeh, M. Shahbazi, A.S. Pakdel, *Corros. Sci*., 92 (2015) 162–172. https://doi.org/10.1016/j.corsci.2014.11.047.
15. N. Van Phuong, K. Lee, D. Chang, M. Kim, S. Lee, S. Moon, *Met. Mater. Int*., 19 (2013) 273–281. https://doi.org/10.1007/s12540-013-2023-0.
16. M.R. El-Sharif, Y.J. Su, C.U. Chisholm, A. Watson, *Corros. Sci*., 35 (1993) 1259–1265. https://doi.org/10.1016/0010-938X(93)90346-I.
17. H.K. Singh, K. V. Yeole, S.T. Mhaske, *Chem. Eng. J*., (2016). https://doi.org/10.1016/j.cej.2016.03.055.
18. D.G. Shchukin, H. Möhwald, *Adv. Funct. Mater*., 17 (2007) 1451–1458. https://doi.org/10.1002/adfm.200601226.
19. M. Costa, C.B. Klein, *Crit. Rev. Toxicol*., 36 (2006) 155–163. https://doi.org/10.1080/10408440500534032.
20. E. Alibakhshi, E. Ghasemi, M. Mahdavian, *Prog. Org. Coatings*., 77 (2014) 1155–1162. https://doi.org/10.1016/j.porgcoat.2014.03.027.
21. Y. Shao, C. Jia, G. Meng, T. Zhang, F. Wang, *Corros. Sci*., 51 (2009) 371–379. https://doi.org/10.1016/j.corsci.2008.11.015.
22. N. Xie, D. Feng, H. Li, C. Gong, L. Zhen, *Mater. Lett.*, 82 (2012) 26–28. https://doi.org/10.1016/j.matlet.2012.05.037.
23. A.J. Jadhav, D. V Pinjari, A.B. Pandit, *Chem. Eng. J*., 297 (2016) 116–120. https://doi.org/10.1016/j.cej.2016.04.001.
24. L. Huang, N. Yi, Y. Wu, Y. Zhang, Q. Zhang, Y. Huang, Y. Ma, Y. Chen, *Adv. Mater*., 25 (2013) 2224–2228. https://doi.org/10.1002/adma.201204768.
25. Y. Uematsu, T. Kitamura, R. Ohtani, *Compos. Sci. Technol*., 53 (1995) 333–341. https://doi.org/10.1016/0266-3538(95)00005-4.
26. S. Yan, W. He, C. Sun, X. Zhang, H. Zhao, Z. Li, W. Zhou, X. Tian, X. Sun, X. Han, *Dye. Pigment*., 80 (2009) 254–258. https://doi.org/10.1016/j.dyepig.2008.06.010.
27. J.D. Wang, D. Li, J.K. Liu, X.H. Yang, J.L. He, Y. Lu, *Soft Nanosci. Lett*., 01 (2011) 81–85. https://doi.org/10.4236/snl.2011.13015.
28. M.A. Djebbi, M. Braiek, P. Namour, A. Ben Haj Amara, N. Jaffrezic-Renault, *Appl. Surf. Sci*., 386 (2016) 352–363. https://doi.org/10.1016/j.apsusc.2016.06.032.
29. A.Q. Yuan, S. Liao, Z.F. Tong, J. Wu, Z.Y. Huang, *Mater. Lett*., 60 (2006) 2110–2114. https://doi.org/10.1016/j.matlet.2005.12.082.
30. M. Crobu, A. Rossi, F. Mangolini, N.D. Spencer, *Anal. Bioanal. Chem*., (2012). https://doi.org/10.1007/s00216-012-5836-7.
31. D. Zhang, Y. Zhao, L. Chen, *Appl. Surf. Sci*., (2018). https://doi.org/10.1016/j.apsusc.2018.07.053.
32. Y. Wu, W. Zhao, W. Wang, W. Sui, *RSC Adv*., 6 (2016) 5100–5110. https://doi.org/10.1039/C5RA25153B.
33. S. Zhou, Y. Wu, W. Zhao, J. Yu, F. Jiang, L. Ma, *Colloids Surf., A*., 556 (2018) 273–283. https://doi.org/10.1016/j.colsurfa.2018.08.045.
34. S. Qiu, W. Li, W. Zheng, H. Zhao, L. Wang, *ACS Appl. Mater. Interfaces*., 9 (2017) 34294–34304. https://doi.org/10.1021/acsami.7b08325.
35. M. Conradi, A. Kocijan, D. Kek-Merl, M. Zorko, I. Verpoest, *Appl. Surf. Sci*., 292 (2014) 432–437. https://doi.org/10.1016/j.apsusc.2013.11.155.

36. S. Pourhashem, M.R. Vaezi, A. Rashidi, M.R. Bagherzadeh, *Corros. Sci.*, 115 (2017) 78–92. https://doi.org/10.1016/j.corsci.2016.11.008.
37. M. Cui, S. Ren, H. Zhao, Q. Xue, L. Wang, *Chem. Eng. J.*, 335 (2018) 255–266. https://doi.org/10.1016/j.cej.2017.10.172.
38. H.H. Hassan, E. Abdelghani, M.A. Amin, *Electrochim. Acta*., 52 (2007) 6359–6366. https://doi.org/10.1016/j.electacta.2007.04.046.
39. S. Qiu, C. Chen, M. Cui, W. Li, H. Zhao, L. Wang, *Appl. Surf. Sci*., 407 (2017) 213–222. https://doi.org/10.1016/j.apsusc.2017.02.142.
40. L.B. Coelho, M.-G. Olivier, *Corros. Sci*., 136 (2018) 292–303. https://doi.org/10.1016/j.corsci.2018.03.015.
41. H. Liu, T. Gu, G. Zhang, Y. Cheng, H. Wang, H. Liu, *Corros. Sci*., 102 (2016) 93–102. https://doi.org/10.1016/j.corsci.2015.09.023.
42. Z.B. Bao, Q.M. Wang, W.Z. Li, J. Gong, T.Y. Xiong, C. Sun, *Corros. Sci*., 50 (2008) 847–855. https://doi.org/10.1016/j.corsci.2007.09.004.
43. B. Ramezanzadeh, M.H. Mohamadzadeh Moghadam, N. Shohani, M. Mahdavian, *Chem. Eng. J*., 320 (2017) 363–375. https://doi.org/10.1016/j.cej.2017.03.061.